JBIC Journal of Biological Inorganic Chemistry (2018) 23:303–312
https://doi.org/10.1007/s00775-018-1535-y

ORIGINAL PAPER

Ibandronate metal complexes: solution behavior and antiparasitic activity

Bruno Demoro[1] · Santiago Rostán[1] · Mauricio Moncada[3] · Zhu-Hong Li[2] · Roberto Docampo[2] · Claudio Olea Azar[3] · Juan Diego Maya[4] · Julia Torres[1] · Dinorah Gambino[1] · Lucía Otero[1]

Received: 15 November 2017 / Accepted: 9 January 2018 / Published online: 18 January 2018

Abstract

To face the high costs of developing new drugs, researchers in both industry and academy are looking for ways to repurpose old drugs for new uses. In this sense, bisphosphonates that are clinically used for bone diseases have been studied as agents against *Trypanosoma cruzi*, causative parasite of Chagas disease. In this work, the development of first row transition metal complexes (M = Co^{2+}, Mn^{2+}, Ni^{2+}) with the bisphosphonate ibandronate (iba, H_4iba representing the neutral form) is presented. The in-solution behavior of the systems containing iba and the selected *3d* metal ions was studied by potentiometry. Mononuclear complexes $[M(H_xiba)]^{(2-x)-}$ (x = 0–3) and $[M(Hiba)_2]^{4-}$ together with the formation of the neutral polynuclear species $[M_2iba]$ and $[M_3(Hiba)_2]$ were detected for all studied systems. In the solid state, complexes of the formula $[M_3(Hiba)_2(H_2O)_4]\cdot 6H_2O$ were obtained and characterized. All obtained complexes, forming $[M(Hiba)]^-$ species under the conditions of the biological studies, were more active against the amastigote form of *T. cruzi* than the free iba, showing no toxicity in mammalian *Vero* cells. In addition, the same complexes were selective inhibitors of the parasitic farnesyl diphosphate synthase (FPPS) enzyme showing poor inhibition of the human one. However, the increase of the anti-*T. cruzi* activity upon coordination could not be explained neither through the inhibition of *Tc*FPPS nor through the inhibition of *Tc*SPPS (*T. cruzi* solanesyl-diphosphate synthase). The ability of the obtained metal complexes of catalyzing the generation of free radical species in the parasite could explain the observed anti-*T. cruzi* activity.

Graphical abstract

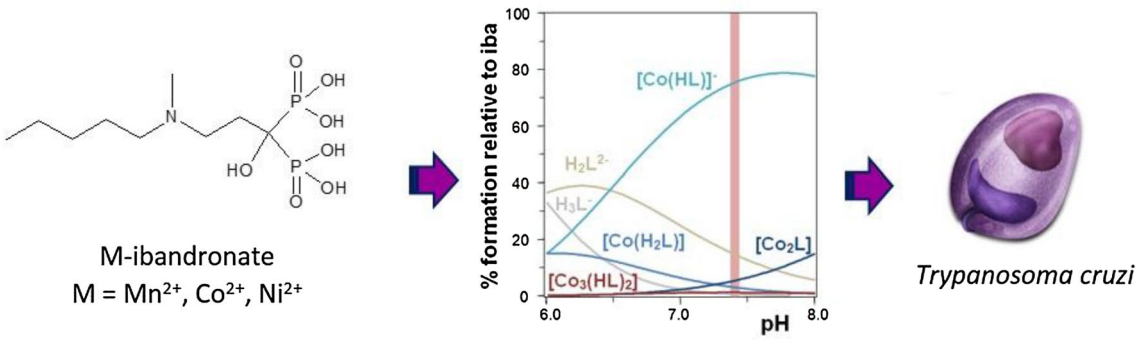

Keywords Ibandronate complexes · Solution studies · *Trypanosoma cruzi*

Introduction

Ibandronate (3-(*N*-methyl-*N*´-penthyl)-amino-1-hydroxypropane-1,1-diphosphonic acid, H_4iba) belongs to the group of nitrogen-containing bisphosphonates (NBP).

Electronic supplementary material The online version of this article (https://doi.org/10.1007/s00775-018-1535-y) contains supplementary material, which is available to authorized users.

Extended author information available on the last page of the article

In these pyrophosphate analogs, the oxygen bridge between the two phosphorus atoms has been replaced by a carbon substituted with various side chains, one of which contains a nitrogen atom (Fig. 1). NBPs are well-established drugs for the prevention and treatment of diseases associated with excessive bone resorption, including Paget's disease of bone, myeloma, bone metastases, and osteoporosis [1–3].

In addition, a number of bisphosphonate derivatives, including ibandronate and many other NBPs, were found to be potent inhibitors of *Trypanosoma cruzi* (*T. cruzi*) proliferation [4, 5]. *T. cruzi* is a protozoan parasite causative of American trypanosomiasis (Chagas disease). This illness used to be confined to the Americas, but over the last two decades it has spread to other continents mainly because of enhanced means of travel and global population movement to and from Latin America. It is estimated that over 10,000 people die every year from clinical manifestations of Chagas disease, and more than 25 million people are under risk of acquiring it [6]. None of the available drugs for the treatment of Chagas disease is satisfactory and new drugs are urgently required. To face the high costs of developing new drugs, one of the approaches used is the repositioning of compounds that were previously developed for an alternative use as new anti-trypanosomatid therapies [7]. Because most repositioned drugs have already passed the early phases of development and clinical testing, they can potentially win approval in less than half the time and at one-quarter of the cost [8, 9]. Based on this approach, commercial NBPs are tested against different parasites, including *T. cruzi*. The selection of NBPs as potential antichagasics is also supported by two main facts. On the one hand, one of the main targets of NBPs is farnesyl diphosphate synthase (FPPS) enzyme. FPPS is a key enzyme of the mevalonate pathway and catalyzes two mandatory biosynthetic steps to form farnesyl pyrophosphate, which is required for the posttranslational prenylation of small binding proteins (among other processes) within both osteoclasts and *T. cruzi* [10–12]. In addition, as acidocalcisomes present in these parasites are equivalent in composition to the bone mineral, accumulation of NBPs into these organelles would facilitate their antiparasitic action [13, 14].

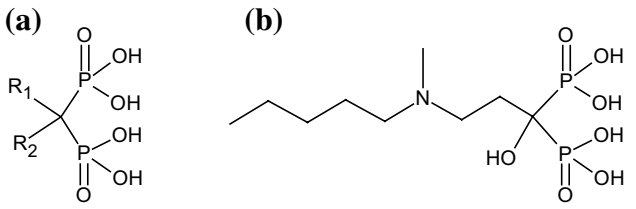

Fig. 1 **a** General structure of bisphosphonates; **b** ibandronate (acid form, H_4iba)

On the other hand, our group had previously developed metal complexes with the NBPs risedronate, alendronate and pamidronate as ligands [15, 16]. Results showed that the coordination of these bisphosphonates to different first row transition metal ions improved their antiproliferative effect against *T. cruzi* exhibiting IC_{50} values against the intracellular amastigote form of the parasite in the low micromolar levels with little toxicity on mammalian *Vero* cells. For these compounds, the increase of the activity and the low toxicity were correlated to a high and selective inhibition of *T. cruzi* farnesyl diphosphate synthase enzyme [15, 16].

Based on these promising results, we expanded our investigations to ibandronate (iba), another bioactive NBP. In this work, we present the synthesis and characterization of three new ibandronate metal complexes of the formula $[M_3(Hiba)_2(H_2O)_4]\cdot 6H_2O$ with M = Co^{2+}, Mn^{2+}, Ni^{2+}. Besides, the interaction of these *3d* metal ions with iba was also studied in solution to predict the predominant species present under the conditions of the biological studies. This approach allowed us to shed light on the potentially active species in the studied systems. The in vitro antiproliferative effect on *T. cruzi* amastigotes and their ability to inhibit both *Trypanosoma cruzi* and human FPPS (*Tc*FPPS and *Hs*FPPS) as well as *Tc*SPPS (*T. cruzi* solanesyl-diphosphate synthase) were evaluated [17]. Finally, the ability of the new complexes of catalyzing the production of free radical species in *T. cruzi* was assessed.

Materials and methods

Materials

All common laboratory chemicals were purchased from commercial sources and were used without further purification. Sodium ibandronate monohydrate ($NaH_3iba\cdot H_2O$) was obtained from Urufarma, Uruguay, including the corresponding certificate of analysis.

Syntheses of $[M_3(Hiba)_2(H_2O)_4]\cdot 6H_2O$ with M = Co^{2+}, Mn^{2+}, Ni^{2+}

$NaH_3iba\cdot H_2O$ (50 mg, 0.14 mmol) was dissolved in 5 mL of water and the solution's pH value was adjusted to 5–6 by addition of NaOH solution. The corresponding amount (0.07 mmol) of $MCl_2\cdot xH_2O$ (with M = Mn, Co, Ni and $x = 4, 6, 6$, respectively) was added. A change in the visible spectra was immediately observed. The obtained solution was heated to 60–70 °C for 20 min. After heating, a microcrystalline solid was filtered off. Alternatively, the same microcrystalline product complex can be isolated at room temperature after 2–3 days.

$[Mn_3(Hiba)_2(H_2O)_4]\cdot 6H_2O$, **Mniba** (yield: 20 mg, 88%) was obtained as a light pink microcrystalline solid. Elemental analysis: found (%): C, 22.08; H, 6.12; N, 2.72; calc. for $C_{18}H_{60}N_2O_{24}P_4Mn_3$: C, 22.12; H, 6.19; N, 2.87. Thermal analysis: 18.9% weight loss corresponding to the elimination of water, compared with a calculated value of 18.4%.

$[Co_3(Hiba)_2(H_2O)_4]\cdot 6H_2O$, **Coiba** (yield: 21 mg, 91%) was obtained as a pink microcrystalline solid. Elemental analysis: found (%): C, 21.87; H, 6.06; N, 2.76. Calc. for $C_{18}H_{60}N_2O_{24}P_4Co_3$: C, 21.86; H, 6.11; N, 2.83. Thermal analysis: 18.8% weight loss corresponding to the elimination of water, compared with a calculated value of 18.2%.

$[Ni_3(Hiba)_2(H_2O)_4]\cdot 6H_2O$, **Niiba** (yield: 15 mg, 65%) was obtained as a green microcrystalline solid. Elemental analysis: found (%): C, 21.76; H, 6.09; N, 2.71. Calc. for $C_{18}H_{60}N_2O_{24}P_4Ni_3$: C, 21.87; H, 6.12; N, 2.83. Thermal analysis: 18.2% weight loss corresponding to the elimination of water, compared with a calculated value of 18.2%.

Physicochemical characterization

C, H and N analyses were carried out with a Thermo Scientific Flash 2000 elemental analyzer. Metal ion content was evaluated by the conventional complexometric technique with EDTA in ammonia buffer solution [18]. UV–Vis spectra were recorded in a Shimadzu 1603 spectrophotometer. The FTIR absorption spectra (4000–400 cm^{-1}) of the complexes and free ligands were measured as KBr pellets with a Shimadzu IR Prestige-21 instrument. Thermogravimetric measurements (TGA) were done on a Shimadzu TGA 50 thermobalance, with a platinum cell, working under flowing nitrogen (50 mL min^{-1}) and at a heating rate of 0.5 °C min^{-1} (RT–80 °C range) and 1.0 °C min^{-1} (80–350 °C range).

Potentiometric titrations

Materials

For potentiometric studies, $MnCl_2\cdot 4H_2O$ from Merck, $CoCl_2\cdot 6H_2O$ from Carlo Erba and $NiCl_2\cdot 6H_2O$ from Merck were used as metal cation sources. All solutions were standardized according to the usual procedure [18]. The standard HCl and NaOH solutions were prepared by diluting Merck standard ampoules. Acid and base stock solutions were standardized against sodium carbonate and potassium hydrogen phthalate, respectively. All the solutions were prepared with analytical grade water (18 μS cm^{-1}) and freed of carbon dioxide by bubbling with Ar(g).

Equilibrium studies

The protonation constants of iba were determined through three potentiometric titrations (ca. 150 experimental points each), in the concentration range 1–3 mM. Then, the behavior of the ligand in the presence of M(II) (M = Mn, Co or Ni) was analyzed through four potentiometric titrations (ca. 100 experimental points each) for each system, at ligand concentrations ranging from 1 to 3 mM, and metal cation to ligand total molar ratios varying from 2:1 to 1:3. A broad pH interval was covered for each titration. Data were collected from ca. 1.5 to 11 pH values. Notwithstanding, data in the 2–10 pH interval were enough to assure detectable proportions of all species.

In each potentiometric experiment, the solutions were poured into a 50-mL titration cell. After thermal equilibrium was reached, hydrogen ion concentrations were determined by successive readings, each performed after a small incremental addition of standard 0.1 M NaOH solution. The titrant addition and e.m.f. measurements were carried out using an automatic titrator Mettler–Toledo DL50-Graphix. The ionic strength was kept almost constant throughout the titrations using solutions containing 0.50 M Me_4NCl and relatively low initial concentrations of metal ions and iba (the sum of these reactants' initial concentrations did not contribute more than 2% on the total ionic strength). Pre-saturated argon (free of CO_2) was bubbled through the solutions during titrations to eliminate the effect of atmospheric carbon dioxide, and the temperature was kept at 25.0 (± 0.1) °C. Equilibrium attainment after each titrant addition was verified by controlling the deviation of successive e.m.f. readings.

Independent stock solutions were used in some titrations to check reproducibility. The cell electrode potential $E°$ and the acidic junction potential were determined according to Ref. [19] from independent titrations of the stock HCl solution with NaOH stock solution. In this way, the pH scale was the free hydrogen concentration scale. The calibration in the alkaline range was checked by recalculating K_w values for each system. The values obtained (average $\log_{10} K_w = 13.78$) were always checked to assure they were in line with reported data under the same experimental conditions [20].

Data were analyzed using the HYPERQUAD program [21], and species distribution diagrams were produced using the HySS program [22]. The fit of the values predicted by the model to the experimental data was estimated on the basis of the σ parameter, corresponding to the scaled sum of squared differences between predicted and experimental values. Final models were selected on the basis of the σ parameter, the model confidence level estimator Chi square, and the internal consistency of data

reflected in standard deviations of the formation constants [21].

Biological studies

Drug screening assays in *Vero* cells and *T. cruzi* intracellular amastigotes

Gamma-irradiated (2000 Rads) Vero cells (3.4×10^4 cells/well) were seeded in 96 well plates (black, clear bottom plates from Greiner Bio-One) in 100 µL RPMI (Roswell Park Memorial Institute from Sigma) with 10% FBS (Fetal Bovine Serum). Gamma irradiation was performed to prevent host cell division and detachment of the culture. Plates were incubated overnight at 35 °C and 7% CO_2. After overnight incubation, Vero cells were challenged with 3.4×10^5 trypomastigotes/well (CL strain overexpressing a tdTomato red fluorescent protein) [23] in 50 µL volume and incubated for 5 h at 35 °C and 7% CO_2. After infection, wells were washed once with Hanks solution (150 µL/well) to eliminate any extracellular parasites and tested compounds were immediately added in serial dilutions in RPMI media in 150 µL volumes and left for the whole period of the experiment. Each dilution was tested in quadruplicate. Each plate also contained controls with host cells and no parasites (for background check), controls with two representative drug dilutions and no parasites (for cytotoxicity assays), and controls with parasites and no drugs (positive control). After drug addition, plates were incubated at 35 °C and 7% CO_2. At day 3 post-infection, plates were assayed for fluorescence. IC_{50} values were determined by non-linear regression analysis using SigmaPlot.

Enzymatic inhibition assays

FPPS assay (for both T. cruzi and human) Human FPPS (*Hs*FPPS) was expressed and purified as previously described [24, 25]. *T. cruzi* FPPS (*Tc*FPPS) was obtained as described before [12]. The FPPS inhibition radiometric assay was performed essentially as previously reported [25]. Briefly, 100 µL of assay buffer (10 mM Hepes (4-(2-hydroxyethyl)-1-piperazineethanesulfonic acid), pH 7.4, 5 mM $MgCl_2$, 2 mM dithiothreitol, 4.7 µM [4-^{14}C] IPP (isopentenyl diphosphate), 10 µCi/µmol, and 55 µM DMAPP (dimethylallyl pyrophosphate) were prewarmed to 37 °C. The assay was initiated by the addition of recombinant protein (10–20 ng). The assay was allowed to proceed for 30 min at 37 °C and was quenched by the addition of 6 M HCl (10 µL). The reaction media were made alkaline with 6.0 M NaOH (15 µL), diluted in water (0.7 mL), and extracted with hexane (1 mL). The hexane solution was washed with water and transferred to a scintillation vial for counting. One unit of enzyme activity was defined as the activity required to incorporate 1 nmol of [4-^{14}C]IPP into [14-^{14}C]FPP (farnesyl diphosphate) in 1 min. IC_{50} values were determined by non-linear regression analysis using SigmaPlot. 10 µL of several dilutions of the complexes were used for the inhibition assay. Positive (no inhibitor, only enzyme) and negative controls (no inhibitor and no enzyme) for each experiment were performed.

TcSPPS assay The activity of the enzyme was determined by a radiometric assay. Briefly, 100 µL of assay buffer (100 mM Tris–HCl buffer, pH 7.4, 1 mM $MgCl_2$, 1% (v/v) Triton X-100, 7.07 µM [4-^{14}C]IPP (10 µCi/lmol)) and 50 µM GGPP (geranylgeranyl diphosphate) were prewarmed to 37 °C. The assay was initiated by the addition of 10–20 ng of recombinant protein. The assay was allowed to proceed for 30 min at 37 °C and was quenched by chilling quickly in an ice bath. The reaction products were extracted with 1 mL of 1-butanol saturated with water. The organic layer was washed with water saturated with NaCl, and transferred to a scintillation vial with 4 mL of scintillation solution Ecolume for counting. One unit of enzyme activity was defined as the activity required to incorporate 1 nmol of [4-^{14}C]IPP into [4-^{14}C]FPP in 1 min [17].

Generation of free radical species in *T. cruzi*

The ability of the new complexes of catalyzing the production of free radical species in *T. cruzi* was assessed in the parasite with ESR (electron spin resonance) using DMPO (5,5-dimethyl-1-pyrroline-*N*-oxide) for spin trapping. Each tested compound was dissolved in DMSO (spectroscopy grade, approx. 1 mM) and the solution was added to a mixture containing the epimastigote form of *T. cruzi* (Dm28c strain; final protein concentration, 4– 8 mg/mL) and DMPO (final concentration, 250 mM). The mixture was transferred to a 50-µL capillary. ESR spectra were recorded in the X band (9.85 GHz) using a Bruker ECS 106 spectrometer with a rectangular cavity and 50-kHz field modulation [26].

Results and discussion

Synthesis and solid-state characterization

Three new metal complexes with ibandronate as ligand have been synthesized and fully characterized. Unlike earlier studies in which high-temperature and -pressure conditions were used in the synthesis of bisphophonate metal compounds [27], complexes of the formula $[M_3(Hiba)_2(H_2O)_4]\cdot 6H_2O$, with M = Mn^{2+}, Co^{2+} and Ni^{2+} were obtained with excellent yields and high purities by direct reaction of aqueous solutions of the ligand and the corresponding metal salts at room temperature. As expected, the yield of the synthetic reaction was highly dependent on the pH value. The highest

yield was observed for Coiba system in the 5–6 pH range, whereas for Mniba and Niiba systems high yields were only obtained for pH values ca. 6. These synthetic conditions are in accordance with the obtained distribution species diagrams calculated for the experimental conditions used to prepare the complexes (see below) in which the neutral species $[M_3(Hiba)_2]$ are present in solution in high concentrations. Since they are neutral species, they are likely to crystallize from the aqueous solution.

The nature of the compounds obtained in the selected synthetic conditions was assessed by the performed solid-state characterizations. Even though NBPs are very versatile ligands that could present different modes of coordination [27], the many X-ray structures reported for first row transition metal complexes with these ligands show similar patterns of coordination and stoichiometries [28–34]. Among them, the 2D-layered structure corresponding to the formula $[M_3(HL)_2(H_2O)_4]\cdot xH_2O$ with HL = monoprotonated form of NBP matches all the performed characterizations for the ibandronate complexes described herein.

On the one hand, analytical data (elemental and thermogravimetric analysis) agreed with the proposed formula. In particular, TGA results performed for all the complexes showed a continuous weigh loss between 45 and 120 °C that agreed with the loss of the total amount of water molecules present in the complexes (ten per complex, see Experimental section). However, in the DTG (derivative thermogravimetry) two broad peaks were distinguished in this temperature range which would be in accordance with the presence of two different water populations. Figure 2 shows the results of the TGA and DTG experiments for Coiba compound as an example. A weight loss of 11.1% at around 50 °C would correspond to the six crystallization water molecules and another weight loss of 7.7% at 95 °C would agree with the presence of four coordinated water molecules in the complex. The weight loss corresponding to each of these two peaks for Niiba and Mniba also agreed with the proposed formula (Figure S1).

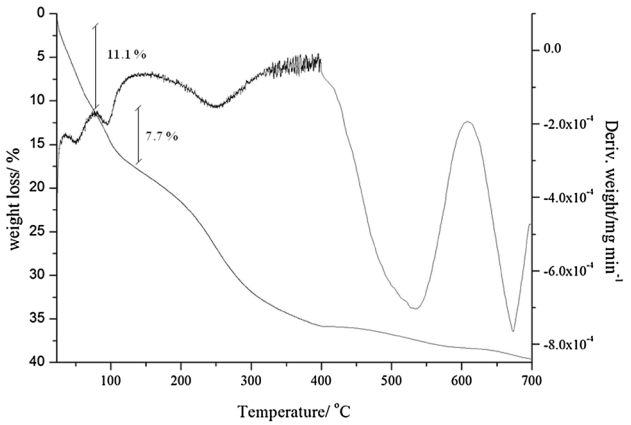

Fig. 2 Thermogravimetric analysis result of Coiba compound

On the other hand, the infrared spectra of the three obtained complexes are almost identical (Figure S2). This is in accordance with all of them being isostructural [15, 16, 32]. In the region of 900–1300 cm^{-1} the obtained compounds show the typical band pattern of phosphonates [15, 16, 32, 35]. In this region, modifications in the frequency values after complex formation could not be clearly attributed to coordination as the presence of water molecules and hydrogen bond formation themselves affect the vibrational spectrum [15, 16, 36]. In the 1100–1250 cm^{-1} region, POO^- stretching bands that are observed at 1195 and 1156 cm^{-1} for ibandronate free ligand are shifted to lower frequencies and collapsed in a broad band at 1061 cm^{-1} in all the Miba metal complexes In addition, the band corresponding to P=O stretching vibrations observed at 1280 cm^{-1} in the free ibandronate ligand is not present in the spectra of all the obtained compounds, indicating that each phosphonate group is fully deprotonated [37]. This is in agreement with the ibandronate ligand coordinating with the metal ion as a zwitterion with both phosphonate groups completely deprotonated and with the basic tertiary N atom in a protonated form, leading to a total charge of − 3 for the coordinated ligand [28, 31, 33, 38]. In addition, the absence of this IR band was previously related to the M–O–P–O–M coordination bridging mode as observed in other $[M_3(HL)_2(H_2O)_4]$ compounds with other NBPs [16, 31, 33]. In these previously reported complexes, the C–OH group was also involved in coordination. However, for the obtained ibandronate complexes, the effect of coordination in the C–O–H stretching band (at 3160 cm^{-1} in the free ligand) was not observed due to the appearance in this region of a wide band that could be assigned to OH stretching of water [15].

Solution studies

Table 1 shows the protonation constants of iba determined in 0.50 M Me_4NCl at 25.0 °C. Iba has four acid protons corresponding to the two phosphonic groups and a basic

Table 1 Logarithms of the overall protonation constants of ibandronate determined in 0.5 M Me_4NCl at 25.0 °C

Protonation equilibrium	log β^H
$iba^{4-} + H^+ \rightarrow Hiba^{3-}$	10.85(6)
$iba^{4-} + 2\ H^+ \rightarrow H_2iba^{2-}$	21.16(5)
$iba^{4-} + 3\ H^+ \rightarrow H_3iba^-$	27.12(6)
$iba^{4-} + 4\ H^+ \rightarrow H_4iba$	29.25(8)
$iba^{4-} + 5\ H^+ \rightarrow H_5iba^+$	30.7(3)

Values given in parentheses are the 1σ statistical uncertainties in the last digit of the constant. $\sigma = 0.6$

tertiary amino group. The first two pK_a values (pK_{a1} = 1.5, pK_{a2} = 2.13) correspond to the first deprotonation of each phosphonic group and thus lie in the strong acid region. Notwithstanding, the experimental determination of these pK values is still reliable since the highly protonated species are present in detectable amounts (for example, for 1 mM total concentration of iba, at pH 2, 14% of the ligand is present as H_5iba^+). pK_{a3} = 5.96 is associated with the release of the second proton from one of the phosphonic groups. The fourth and fifth pK_a values (pK_{a4} = 10.31, pK_{a5} = 10.85) are related to the last deprotonation of the bis(phosphonic acid) moiety and the deprotonation of the amino group, respectively. These results are in line with previously reported data on NBP and other bisphosphonates [38–45]. Figures S3 and S4 show the fitting of experimental data and the corresponding distribution species diagram of iba in the absence of metal ions.

Table 2 shows the obtained results for the interaction of iba with the selected *3d* metal ions. Mononuclear complexes, $[M(H_xiba)]^{(2-x)-}$ (x = 0–3), together with $[M(Hiba)_2]^{4-}$, $[M_2iba]$ and $[M_3(Hiba)_2]$ are detected for all studied systems. The stability constant values are very similar for all +2 metal cations. Figure 3a shows distribution species diagram for one typical potentiometric titration ($[iba]_{total}$ = 2 mM, $[Co]_{total}$ = 1 mM). Similar diagrams are obtained for Mn(II) and Ni(II) under the same experimental conditions (see Figures S5 and S6), An example of the experimental fit of data for Coiba system is also shown as Figure S7. The species $[M(H_xiba)]^{(2-x)-}$ with the ligand under different degrees of protonation have already been reported for other NBPs [38–40, 42]. In the case of $[M(H_3iba)]^+$, only one previous report informed the detection of a species with the same stoichiometry for other NBPs in the acidic region [42]. It is worth mentioning that the measured visible spectra supports complexation at this very low pH interval (results not shown) giving further evidence of the formation of $[M(H_3iba)]^+$ in solution. Together with 1:1 species, $[M(Hiba)_2]^{4-}$, $[M_2iba]$ and $[M_3(Hiba)_2]$ are formed. Some previous reports have also detected similar species for other NBPs [38–40, 42]. Their formation is favored when the reagents are not in equimolar amounts and for higher total concentrations, especially for the trinuclear complex. In fact, under the conditions of the synthesis, $[M_3(Hiba)_2]$ becomes the predominant form of Co(II) (Fig. 3b), in line with the isolation of the solid compound bearing the same stoichiometry. For Mn or Ni, $[M_3(Hiba)_2]$ is also present in lower proportion under the conditions used in the synthetic procedures, together with $[M(H_2iba)]$. This is in agreement with the lower yield observed for Mn and Ni solid compounds together with the fact that better results are obtained if pH value is fixed at six instead of five (Figures S8 and S9).

Besides the synthesis conditions, it is also relevant to know which is the most abundant Miba species in the conditions of the biological studies. Figure 4 shows the distribution species diagram calculated for the concentration range of the biological studies regarding anti-*T. cruzi* activity (Sect. 3.3). Taking Coiba system as example, at pH 7.4 in the solution prepared from the solid Coiba compound,

Table 2 Logarithms of the formation constants of M(II)–ibandronate in 0.5 M Me_4NCl at 25.0 °C

Equilibrium	Mn	Co	Ni
$M^{2+} + iba^{4-} \rightarrow [M(iba)]^{2-}$	8.52(8)	9.42(5)	9.29(8)
$M^{2+} + iba^{4-} + H^+ \rightarrow [M(Hiba)]^-$	19.45(8)	19.68(5)	19.41(7)
$M^{2+} + iba^{4-} + 2\ H^+ \rightarrow [M(H_2iba)]$	26.56(7)	25.68(4)	25.52(6)
$M^{2+} + iba^{4-} + 3\ H^+ \rightarrow [M(H_3iba)]^+$	30.99(8)	30.36(4)	30.25(7)
$M^{2+} + 2\ iba^{4-} + 2\ H^+ \rightarrow [M(Hiba)_2]^{4-}$	33.51(8)	33.7(1)	33.86(9)
$2\ M^{2+} + iba^{4-} \rightarrow [M_2iba]$	15.0(1)	16.34(8)	15.45(9)
$3\ M^{2+} + 2\ iba^{4-} + 2\ H^+ \rightarrow [M_3(Hiba)_2]$	48.8(2)	47.58(8)	46.0(1)
σ	0.8	1.0	0.7

Tabulated values are the overall formation constant of each species. Values given in parentheses are the 1σ statistical uncertainties in the last digit of the constant

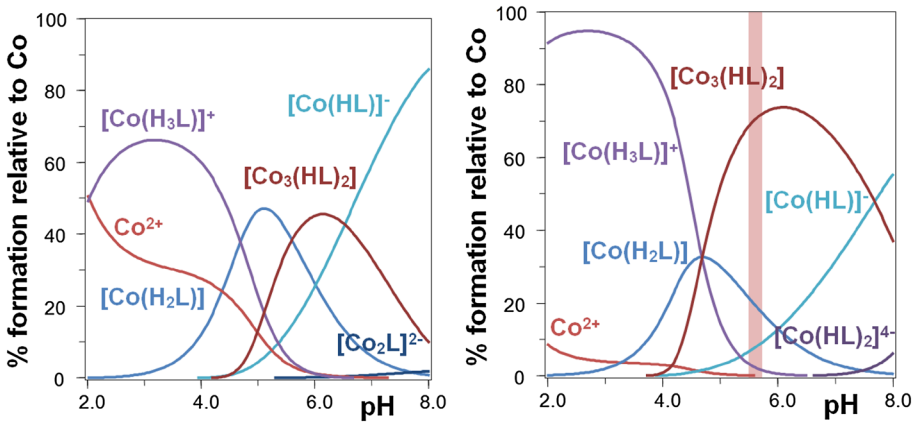

Fig. 3 Distribution species diagram of Coiba system calculated from equilibrium constants in Tables 1 and 2. *L* represents the fully deprotonated form of iba. Conditions: 0.5 M Me_4NCl, 25.0 °C. **a** Potentiometric experimental conditions: $[Co]_{total}$ = 1 mM, $[iba]_{total}$ = 2 mM; **b** synthesis conditions: $[Co]_{total}$ = 15 mM, $[iba]_{total}$ = 30 mM, pH interval is indicated

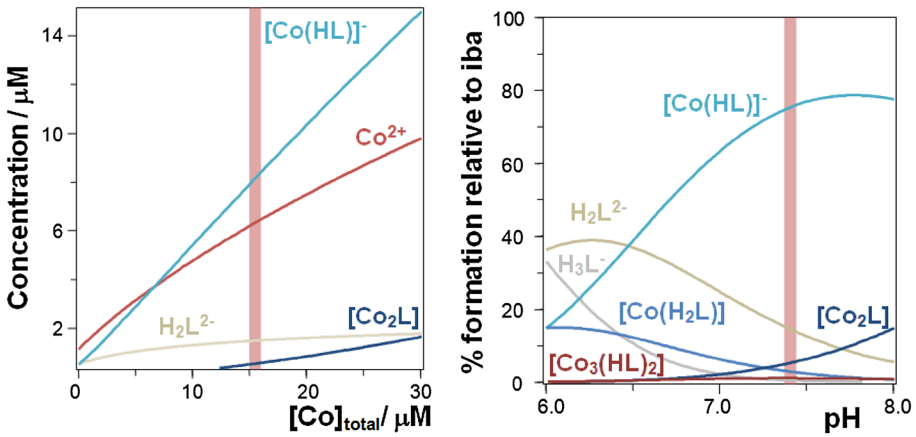

Fig. 4 Distribution species diagram of Coiba system calculated from equilibrium constants in Tables 1 and 2. *L* represents the fully deprotonated form of iba. Conditions: 0.5 M Me_4NCl, 25.0 °C. Conditions: **a** pH 7.4, $[Co]_{total}$ = 1.8–30 μM, $[iba]_{total}$ = 1.2–20 μM, IC_{50} interval is indicated; **b** IC_{50} concentrations corresponding to $[Co]_{total}$ = 15.6 M, $[iba]_{total}$ = 10.4 μM

the most abundant complex species is $[M(Hiba)]^-$ for all the concentration intervals used in the experiments (Fig. 4a). Free Co^{2+} and H_2iba^{2-} are also present under these conditions. Since neither the free metal ion nor the free ligand are active against *T. cruzi*, the species $[M(Hiba)]^-$ seems to be responsible for the observed behavior. For the IC_{50} concentrations (Fig. 4b), the calculated concentration of the $[Co(Hiba)]^-$ complex in solution is 7.8 μM, retaining 75% of the ligand. Similar results are obtained for the other employed *3d* metal ions. Figures S10 and S11 show the predominance of $[M(Hiba)]^-$ complex for the IC_{50} concentrations with concentrations of 6.3 μM of $[Mn(Hiba)]^-$ (39% of the ligand) and 3.2 μM of $[Ni(Hiba)]^-$ (62% of the ligand).

Biological results

The activity against intracellular amastigote forms of *T. cruzi* of ibandronate and the obtained metal complexes was studied. Results are shown in Table 3. In the assayed conditions, the free ibandronate ligand does not show any activity against the amastigote form of *T. cruzi*. However, all obtained complexes were potent inhibitors of *T. cruzi*'s growth having IC_{50} values in the low micromolar range. The antiparasitic activity arises as a consequence of metal complexation and it seems to be quite independent of the nature of the metal ion. It also should be noted that Miba complexes showed no toxicity on the mammalian Vero cells in all the assayed conditions. An increase in the anti-*T. cruzi* activity has previously been reported by us for other metal–bisphosphonate complexes [15, 16].

Insight into the mechanism of action

*Tc*FPPS inhibition assay

The main mechanism of anti-*T. cruzi* action of bisphosphonates and their metal complexes has been related to the inhibition of *Tc*FPPS enzyme [13, 15, 16]. In addition, it has been stated that magnesium ions are necessary for the binding of bisphosphonates to FPPS [46]. Metal (II) ions present in the obtained metal complexes could be responsible for an improved binding ability to FPPS and hence to the improved activity. Both Mg(II) and the transition metal ions form very similar species in solution in the presence of NBPs. In the case of transition metal cations, the interaction with NBPs is stronger [40, 42] supporting the possible substitution of the alkaline earth metal ion by Mn, Co or Ni. Therefore, the ability of the obtained ibandronate complexes

Table 3 Results of biological assays performed with the obtained metal bisphosphonate complexes

Compound	IC_{50} (μM)[a] (amastigotes)	IC_{50} (μM)[b] (*Tc*FPPS)	IC_{50} (μM)[c] (*Hs*FPPS)	IC_{50} (μM)[d] (*Tc*SPPS)
Ibandronate	> 100	0.19 ± 0.04	0.96 ± 0.09	1.22 ± 0.51
Mniba	8.1 ± 3.8	0.06 ± 0.01	> 10	2.18 ± 0.42
Coiba	5.2 ± 0.8	0.42 ± 0.08	> 10	2.69 ± 1.26
Niiba	2.6 ± 1.9	0.07 ± 0.01	5.6 ± 0.9	1.29 ± 0.28
Benznidazole	1.9 ± 0.6	–	–	–

[a]Concentration of compounds inhibiting 50% growth of *T. cruzi* amastigotes

[b]Concentration of compounds inhibiting 50% activity of *Tc*FPPS

[c]Concentration of compounds inhibiting 50% activity of *Hs*FPPS

[d]Concentration of compounds inhibiting 50% activity of *Tc*SPPS

to inhibit *Tc*FPPS was assayed. Results are depicted in Table 3. All metal complexes were inhibitors of *Tc*FPPS. In two cases (Mniba, Niiba) the IC_{50} values were lower than that observed for the free ibandronate ligand. For other previously obtained bisphosphonate metal compounds, a fairly good correlation between the ability of the complexes to inhibit intracellular *T. cruzi* amastigotes' growth and *Tc*FPPS activity had been found. However, for the ibandronate complexes described herein, *Tc*FPPS inhibition values could not explain the increase of the anti-*T. cruzi* activity as a consequence of metal complexation. This apparent lack of correlation between the trypanocidal activity and the enzymatic inhibition by some of the compounds could suggest other potential targets.

*Tc*SPPS inhibition assay

Solanesyl-diphosphate synthase is an enzyme belonging to the prenyltransferase family involved in the biosynthesis of solanesyl diphosphate, a precursor of the side chains of ubiquinones. Because ubiquinones play a central role in energy production in parasites, *Tc*SPPS could be a promising chemotherapeutic target, in particular for bisphosphonates [17]. Results of the inhibition of *Tc*SPPS for ibandronate and the obtained metal complexes are shown in Table 3. Both the free ligand and the metal complexes show a similar level of inhibition of *Tc*SPPS. Therefore, the inhibition of this enzyme could not either explain the increase of the anti-*T. cruzi* activity upon coordination.

HsFPPS inhibition assay

Ibandronate and all obtained complexes were also assayed on their ability to inhibit *Hs*FPPS (Table 3) to study their selectivity of the antiparasitic action. Ibandronate showed fairly poor selectivity as IC_{50} value for the inhibition of *Hs*FPPS is only five times higher than that of *Tc*FPPS. However, ibandronate metal complexes are selective inhibitors of *Tc*FPPS showing selectivity indexes of nearly 100 in most cases. These results can be correlated with the observed lack of toxicity on mammalian Vero cells for the obtained complexes.

Intraparasitic detection of free radical species

To find an explanation for the high anti-*T. cruzi* activity of the ibandronate metal compounds, their ability to catalyze the intraparasitic production of free radical species through Fenton-like reactions was studied. M(II) metal ions present in the obtained complexes could catalyze these reactions as Fe(II) usually does [47]. In this line, compounds were incubated with *T. cruzi* (Dm28c strain) epimastigotes and the production of free radicals was assessed by ESR. DMPO was added to the solutions to trap possible intracellular free radical species having short half-lives. A common pattern of signals was observed for the three complexes on the ESR spectra (Fig. 5). Even though not all signals could be assigned, the triplet corresponding to the oxidized form of DMPO (DMPOX, $a_N = 14.8$ G) was unequivocally detected. As it has been previously reported [48, 49], DMPO oxidation reaction would be caused by the previous generation of DMPO-OH spin adduct that readily derives into the oxidized form of DMPO (Fig. 5, inset). Based on these results, the increased anti-*T. cruzi* activity of the obtained compounds could be related to their ability to produce potentially toxic radical species in the parasite.

Conclusions

Three new *3d* metal complexes with ibandronate as ligand were synthesized and fully characterized. In solution, mononuclear complexes $[M(H_xiba)]^{(2-x)-}$ (x = 0-3) and $[M(Hiba)_2]^{4-}$ together with the formation of the polynuclear species $[M_2(iba)]$ and $[M_3(Hiba)_2]$ were detected for all studied systems (M = Mn^{2+}, Co^{2+} and Ni^{2+}). Under the conditions of the synthesis, $[M_3(Hiba)_2]$ predominates in solution giving place to the isolation of the solid compounds $[M_3(Hiba)_2(H_2O)_4]\cdot 6H_2O$. The complex species $[M(Hiba)]^-$, predominantly formed under the conditions of the anti-*T. cruzi* activity studies is proposed as the active

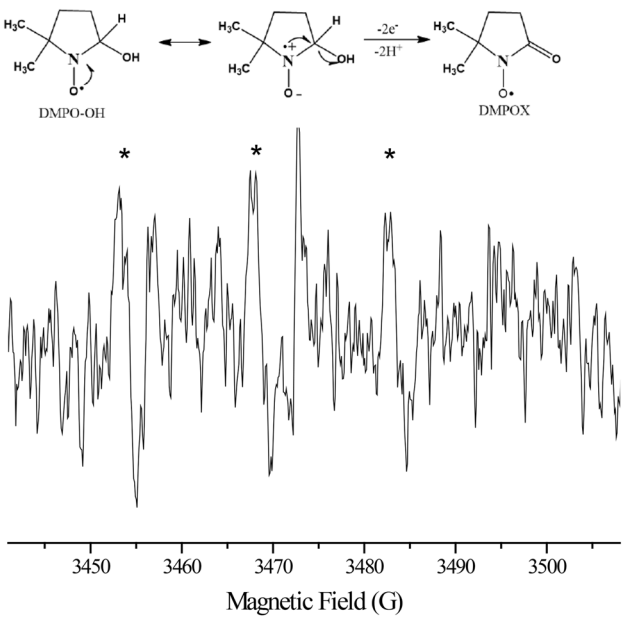

Fig. 5 Experimental ESR spectra obtained after 5 min incubation of Coiba (1 mM) with *T. cruzi* epimastigotes (Dm28c strain, final protein concentration 4–8 mg/mL), NADPH (1 mM), and DMPO (100 mM). Asterisk (*) characteristic signals of DMPOX species. Inset: mechanism of DMPOX generation

species. Regardless the metal ion, the obtained IC_{50} values for the growth inhibition of the amastigote form of *T. cruzi* fell into the low micromolar range even though no activity was observed for the free ibandronate ligand. The increase of the anti-*T. cruzi* activity upon coordination could not be explained neither through the inhibition of *Tc*FPPS nor through the inhibition of *Tc*SPPS even though obtained complexes were selective inhibitors of *Tc*FPPS showing poor inhibition of the human one. The ability of the obtained metal complexes of catalyzing the generation of free radical species in the parasite could be related to the observed anti-*T. cruzi* activity.

Acknowledgements We thank Melina Galizzi for technical help. BD thanks ANII (Uruguay) for the doctoral grant. Authors thank PEDECIBA and ANII-SNI, Uruguay, and FONDECYT 1150175 and URC-024/16, Chile. This work was supported in part by the US National Institutes of Health (Grant AI107633 to RD).

References

1. Malpezzi L, Giordano Carcano EM, Ventimiglia G (2012) J Therm Anal Calorim 109:373–379
2. Graham Russell R (2011) Bone 49:2–19
3. Gatti D, Adami S, Viapiana O, Rossini M (2015) Expert Opin Pharmacother 16(16):2409–2421
4. Docampo R, Moreno SNJ (2001) Curr Drug Targets 1:51–61
5. Urbina JA, Docampo R (2003) Trends Parasitol 19:495–501
6. World Health Organization. http://www.who.int/chagas/disease/en/. Accessed 20 May 2017
7. Field MC, Horn D, Fairlamb AH, Ferguson MAJ, Gray DW, Read KD, De Rycker I, Torrie LS, Wyatt PG, Wyllie S, Gilbert IH (2017) Nat Rev Microbiol 15:217–231
8. Strittmatter SM (2014) Nat Med 20(6):590–601
9. Jin G, Wong ST (2014) Drug Discov Today 19(5):637–644
10. Cheng F, Oldfield E (2004) J Med Chem 47(21):5149–5158
11. Rondeau JM, Bitsch F, Bourgier E, Geiser M, Hemmig R, Kroemer M, Lehmann S, Ramage P, Rieffel S, Strauss A, Green JR, Jahnke W (2006) Chem Med Chem 1:267–273
12. Montalvetti A, Bailey BN, Martin MB, Severin GW, Oldfield E, Docampo R (2001) J Biol Chem 276:33930–33937
13. Docampo R, Moreno SNJ (2008) Curr Pharm Des 14:882–888
14. Urbina JA, Moreno B, Vierkotter S, Oldfield E, Payares G, Sanoja C, Bailey BN, Yan W, Scott DA, Moreno SNJ, Docampo R (1999) J Biol Chem 274:33609–33615
15. Demoro B, Caruso F, Rossi M, Benítez D, Gonzalez M, Cerecetto H, Parajón-Costa B, Castiglioni J, Gallizi M, Docampo R, Otero L, Gambino D (2010) J Inorg Biochem 104:1252–1258
16. Demoro B, Caruso F, Rossi M, Benítez D, González M, Cerecetto H, Galizzi M, Malayil L, Docampo R, Faccio R, Mombrú AW, Gambino D, Otero L (2012) Dalton Trans 41(21):6468–6476
17. Ferella M, Montalvetti A, Rohloff P, Miranda K, Fang J, Reina S, Kawamukai M, Búa J, Nilsson D, Pravia C, Katzin A, Cassera MB, Åslund L, Andersson B, Docampo R, Bontempi EJ (2006) J Biol Chem 281(51):39339–39348
18. Schwarzenwach G, Flaschka H (1969) Complexometric titrations, 2nd edn. Methuen, London
19. Gans P, O'Sullivan B (2000) Talanta 51:33–37
20. IUPAC Stability Constants Database (2007) Academic Software, UK
21. Gans P, Sabatini A, Vacca A (1996) Talanta 43:1739–1753
22. Alderighi L, Gans P, Ienco A, Peters D, Sabatini A, Vacca A (1999) Coord Chem Rev 184:311–318
23. Canavaci AM, Bustamante JM, Padilla AM, Pereza Brandan CM, Simpson LJ, Xu D, Boehlke CL, Tarleton RL (2010) PLOS Negl Trop Dis 4:e740–e745
24. Kavanagh KL, Guo K, Dunford JE, Wu X, Knapp S, Ebetino FH, Rogers MJ, Russell RG, Oppermann U (2006) Proc Natl Acad Sci USA 103:7829–7834
25. Rilling HC (1985) Methods Enzymol 110:145–152
26. Cipriani M, Toloza J, Bradford L, Putzu E, Vieites M, Curbelo E, Tomaz AI, Garat B, Guerrero J, Gancheff JS, Maya JD, Olea Azar C, Gambino D, Otero L (2014) Eur J Inorg Chem 27:4677–4689
27. Matczak-Jon E, Videnova-Adrabinska V (2005) Coord Chem Rev 249:2458–2488
28. Pui Man S, Motevalli M, Gardiner S, Sullivan A, Wilson J (2006) Polyhedron 25:1017–1032
29. Hesham HA, Gil-Hernández B, Abu-Shandi K, Sanchiz J, Janiak C (2010) Polyhedron 29(12):2537–2545
30. Zhang Z, Bao S, Zheng L (2007) Inorg Chem Commun 10:1063–1066
31. Zhang Z, Zheng LM (2008) Inorg Chem Commun 11:1243–1245
32. Gong Y, Tang W, Hou W, Zha Z, Hu C (2006) Inorg Chem 45:4987–4995
33. Cao D, Li Y, Zheng L (2007) Inorg Chem 46:7571–7578
34. Sun Z, Mao J, Dong Z (2005) Polyhedron 24:571–577
35. Redman-Furey N, Dicks M, Bigalow-Kern A, Thomas Cambron R, Lubey G, Lester C, Vaughn D (2005) J Pharm Sci 94(4):893–911
36. Juribašić M, Tušek-Božić L (2009) J Mol Struct 924–926:66–72
37. Melánová K, Beneš L, Svoboda J, Zima V, Trchová M, Vlček M, Almonasy N (2017) J Incl Phenom Macrocycl Chem 87:331–339
38. Kurzak B, Goldeman W, Szpak M, Matczak-Jon E, Kamecka A (2015) Polyhedron 85:675–684
39. Matczak-Jon E, Kurzak B, Kamecka A, Kafarski P (2002) Polyhedron 21:321–332
40. Matczak-Jon E, Kurzak B, Kafarski P, Wozna A (2006) J Inorg Biochem 100:1155–1166
41. Gumienna-Konteck E, Jeziersk J, Lecouvey M, Leroux Y, Kozlowski H (2002) J Inorg Biochem 89:13–17
42. Kubícek V, Kotek J, Hermann P, Lukes I (2007) Eur J Inorg Chem 2007:333–344
43. Deluchat V, Bollinger J, Serpaud B, Caullet C (1997) Talanta 44:897–907
44. Bouhsina S, Bugly P, Abi Aad E, Aboukais A, Kiss T (2004) Inorg Chim Acta 357:305–310
45. Bentouhami E, Bouet GM, Khan MA (2002) Talanta 57:545–554
46. Yokoyama T, Mizuguchi M, Ostermann A, Kusaka K, Niimura N, Schrader TE, Tanaka I (2015) J Med Chem 58:7549–7556
47. Valavanidis A, Vlahoyianni T, Fiotakis K (2005) Free Radic Res 39(10):1071–1081
48. Lawrence A, Jones CM, Wardman P, Burkitt MJ (2003) J Biol Chem 278:29410–29419
49. Aguilera-Venegas B, Olea-Azar C, Arán V, Maya JD, Kemmerling U, Speisky H, Mendizábal F (2012) Int J Electrochem Sci 7:5837–5863

Affiliations

Bruno Demoro[1] · Santiago Rostán[1] · Mauricio Moncada[3] · Zhu-Hong Li[2] · Roberto Docampo[2] · Claudio Olea Azar[3] · Juan Diego Maya[4] · Julia Torres[1] · Dinorah Gambino[1] · Lucía Otero[1]

✉ Lucía Otero
luotero@fq.edu.uy

[1] Química Inorgánica, Facultad de Química, Universidad de la República, Gral. Flores 2124, 11800 Montevideo, Uruguay

[2] Center for Tropical and Emerging Global Diseases and Department of Cellular Biology, University of Georgia, Athens, USA

[3] Departamento de Química Inorgánica y Analítica, Facultad de Ciencias Químicas y Farmacéuticas, Universidad de Chile, Santiago, Chile

[4] ICBM, Facultad de Medicina, Universidad de Chile, Santiago, Chile